PERGAMON

International Journal of Solids and Structures 37 (2000) 1045–1063

INTERNATIONAL JOURNAL OF SOLIDS and STRUCTURES

www.elsevier.com/locate/ijsolstr

Finite element analysis of the wedge delamination test

M. Schulze[a,*], W.D. Nix[b]

[a]*Fraunhofer-Institut für Werkstoffmechanik, Wöhlerstr. 11, D-79108 Freiburg, Germany*
[b]*Department of Materials Science and Engineering, Stanford University, Stanford CA 94305-2205, USA*

Received 9 March 1998; in revised form 17 September 1998

Abstract

The wedge delamination test has been investigated using the finite element method (FEM). Results of the FEM for the deformation behavior of a soft uncoated substrate have been compared with a widely used analytical model. Furthermore, the effect of the presence of a thin hard coating attached to the surface of the soft substrate on the deformation behaviour has been presented. Special attention has been given to the strains and stresses within the coating and to the calculation of the energy release rate in the case of a coating delamination. It was possible to show that analytical calculations of the energy release rate based on uncoated substrates are in good agreement with the finite element calculations of coated substrates despite the fact that locally the deformation behavior at the surface of the substrate can be quite different for both cases.

1. Introduction

Coated specimens are used in many applications where a single component can not meet the design requirements. These applications include aerospace and automotive applications, micromechanics, and microelectronics. The advantage gained by selecting a coating with attractive material properties may be accompanied by the risk of poor adhesion between the coating and the substrate. An unexpected coating delamination can lead to complete failure of the work piece, even though the coating and substrate materials fully meet the requirements of the application. Therefore, knowledge about the adhesion between the coating and substrate materials is of prime importance.

In practice, there exist many methods to investigate adhesion strength (Mittal, 1995). Unfortunately, most methods are useful only for a very limited range of applications. In the case of very well adhering materials, the scratch test has been widely used (Schulze, 1996). However, the attractive ability of the scratch test to debond even very adherent coatings from the substrate is diminished by the often difficult interpretation of the test results.

* Corresponding author: Siemens AG, ZT PA Z, P.O. Box 22 16 34, D-80506 Munich, Germany; fax: 00 49 89 636 81821.
E-mail address: mark.schulze@mchm.siemens.de (M. Schulze)

0020-7683/00/$ - see front matter
PII: S0020-7683(98)00285-6

The wedge delamination test, on the other hand, gives the advantage of having a well defined loading condition. In contrast to the indentation test using a Rockwell-C indenter (Drory and Hutchinson, 1994), the wedge delamination test does not induce tensile radial stresses. Rather the wedge test creates compressive stresses parallel to the surface so that the creation of cracks in the coating is suppressed. The wedge delamination test has been successfully applied by Vlassak et al. (1997) to the well-adhering systems of titanium substrates that are coated with diamond films. From experimental data, Vlassak calcuated the strains at the interface between the substrate and coating using an analytical model. From that he calculated the energy release rate for coating delamination.

In the present work the wedge delamination test of a coating-substrate system is simulated by the means of the finite element method. It is investigated how well the analytical model is in agreement with the finite element simulations for uncoated and coated substrates and, where possible, with experimental data.

2. Wedge indentation

2.1. Theory

In the wedge delamination test used by Vlassak (1997) a wedge with a triangular cross section is pressed deeply (indentation depth $d \gg$ coating thickness t) into a specimen that is composed of a ductile substrate and a hard coating (Fig. 1). This is identical to an indentation in a plane strain condition. The origin of the cartesian coordinate system is set at the point of first contact within the (x, y)-plane. The wedge is displaced along the negative y-axis.

Outside the contact area the surface is displaced in the x-direction. It is assumed that the coating is so thin that it has no influence over the deformation behavior of the overall system. In this case the strains in the interface are governed by the deformation of the substrate alone. Under the assumptions that

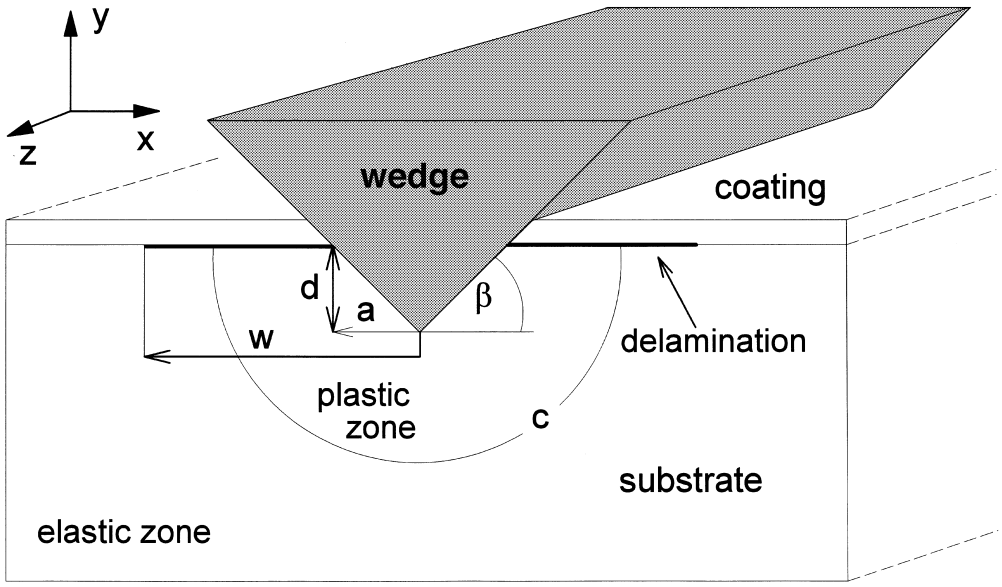

Fig. 1. Sketch of the wedge indentation..

- the substrate can be described by elastic-plastic material behavior with Tresca's flow criterion and without strain hardening, and that
- the elastic compressibility in the plastic zone around the indentation is neglected as a first approximation,

the (radial) displacement $u(x)$ along the x-axis at the surface in the elastic zone is

$$u(x) = \left(\frac{1+v}{E}\right)_s \frac{Y}{2}\frac{c^2}{x} \tag{1}$$

where v is Poisson's ratio, E is Young's modulus, Y is the yield stress, c is the radius of the plastic zone and x is the radial distance to the plane of symmetry (see Fig. 1); the subscript 's' denotes substrate properties (Hill, 1950; Johnson, 1970; Timoshenko and Goodier, 1987). The plastic zone is centered at the line of first contact. If the material within the plastic zone is incompressible, it follows that

$$c = a\sqrt{\frac{2\tan(\beta)E}{\pi(1+v)Y}} \tag{2}$$

where a is half the width of the indentation, and β is the inclination of the face of the wedge to the x-axis (see Fig. 1). The radial displacements within the plastic zone are calculated in a similar fashion, they yield the same expressions as the displacements within the elastic zone. From eqns (1) and (2) the displacement $u(x)$ and the strains on the whole surface outside the contact zone are calculated as

$$u(x) = \frac{a^2\tan(\beta)}{\pi x}, \quad \varepsilon_{xx} = \frac{du}{dx} = -\frac{a^2\tan(\beta)}{\pi x^2}, \quad \Delta\varepsilon_{zz} = 0. \tag{3}$$

In this model the strains at the surface of the substrate are identical to the strains at the interface, and, accordingly, they also describe the behavior of the thin film. The stresses within the film can be calculated using Hooke's law:

$$\sigma_{xx} = -\left(\frac{E}{1-v^2}\right)_{\text{film}} \frac{a^2\tan(\beta)}{\pi x^2}, \quad \sigma_{zz} = v_{\text{film}}\sigma_{xx}. \tag{4}$$

where the subscript 'film' denotes coating properties. If a biaxial residual stress σ_{res} exists, it is added to both stress components in eqn (4). The coating thickness t is assumed to be so small that the stress components are constant over t. If locally the strain energy density W that is stored within the coating, i.e.

$$W = \sum_{ij}\frac{1}{2}\int \sigma_{ij}\,\mathrm{d}\varepsilon_{ij}, \tag{5}$$

is sufficiently large, parts of the coating will detach from the substrate up to $x = w$, where w denotes the half width of the delaminated area (Fig. 1). The detached coating can still be connected to the adherent part of the coating. In this case σ_{xx} in the detached region relaxes to zero and a stress component in the z-direction with a value of $\sigma_{zz} - v_{\text{film}}\,\sigma_{xx}$ remains.

For this fracture mechanics problem in plane strain the energy release rate G can be calculated as the difference between the strain energy density W_1 in front and W_2 behind the crack tip, multiplied by the coating thickness t (Drory and Hutchinson, 1994):

$$G = t(W_1 - W_2) = \frac{\left(1 - v_{\text{film}}^2\right)}{2E_{\text{film}}}\sigma_{xx}^2 t, \tag{6}$$

with

$$W_1 = \frac{\sigma_{xx}^2}{2E_{\text{film}}} + \frac{\sigma_{zz}^2}{2E_{\text{film}}} - \frac{v_{\text{film}}\sigma_{xx}\sigma_{zz}}{E_{\text{film}}}, \quad W_2 = \frac{(\sigma_{zz} - v_{\text{film}}\sigma_{xx})^2}{2E_{\text{film}}}. \tag{7}$$

It is assumed that the energy released is consumed by the coating delamination and that the coating thickness is much smaller than the typical value of the indentation displacement. This guarantees that locally a steady state at the crack front is reached.

For a more realistic indentation it can be expected that within the plastic zone the deformation is constrained by the surrounding material and thus elastic effects influence the deformation behavior. Taking this into account the displacement field can be calculated (Hill, 1950), resulting in an expression for the radial displacement $u(x)$ at the surface, i.e.

$$u(x) = \sqrt{\frac{B\left(C^{2(A+1)} - x^{2(A+1)}\right) + (x + u_{el})^2(A+1)x^{2A}}{(A+1)c^{2A}}} - x \tag{8}$$

with

$$c = a\sqrt{\frac{4\tan(\beta)E_{\text{s}}}{(5 - 4v_{\text{s}})\pi Y}}, \quad A = \frac{3(1 - 2v_{\text{s}})Y}{2E_{\text{s}}}$$

$$B = \frac{(5 - 4v_{\text{s}})Y}{2E_{\text{s}}}, \qquad u_{\text{el}} = \frac{(1 + v_{\text{s}})Yx}{2E_{\text{s}}} \tag{9}$$

If pile-up is taken into account, the displacements can not be calculated analytically. Still, if the pile-up can be measured experimentally one can make an approximation to incorporate it by replacing the theoretically calculated (half) contact width a, i.e. without pile-up, by an effective contact width a_{eff} (Vlassak et al., 1997):

$$a_{\text{eff}} = a\sqrt{\frac{V_0 - V_{\text{pile-up}}}{V_0}}, \tag{10}$$

where $V_{\text{pile-up}}$ is the volume of the pile-up, and V_0 is the volume displaced by the indentation. All equations remain valid, and the radius c of the plastic zone and the energy release rate G are reduced accordingly. To gain a realistic picture of the deformation behavior in the presence of a pile-up other methods like the finite element methods must be used.

It should be stressed that strain hardening of the substrate and friction have not been incorporated in this model.

2.2. Finite element modelling

To realistically simulate the wedge indentation test the finite element method is used (Bathe, 1986; Zienkiewicz, 1977). For the modelling—using the finite element packages MARC and ABAQUS—the following assumptions are made:

- Fractured pieces of the coating within the contact area that may not have delaminated from the

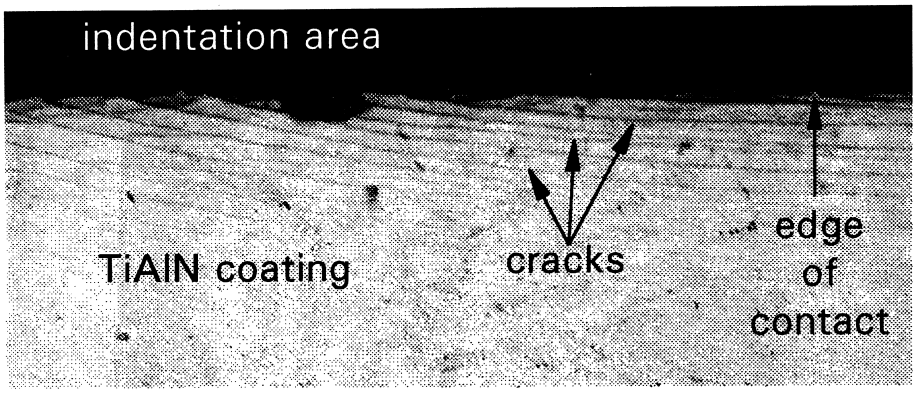

Fig. 2. Microscopic picture of a TiA1N coating on steel after a wedge indentation.

substrate do not significantly influence the indentation. These pieces could originate from the beginning of the indentation process and would crack very fast due to high tensile stresses. Since they are fractured they do not transmit forces on the surface and are subsequently neglected. This picture is especially valid for large indentation depths as used in this simulation where $d \gg t$. Fig. 2 shows tensile cracking of a TiA1N coating on steel along the edge of the contact area. Consequentially, there is no coating modelled within the contact area.

- The indenter is rigid. Experimentally, a deformation of the indenter will occur. If the substrate is sufficiently soft, this deformation is limited to a small region around the sharp corner of the wedge. The larger the indentation depth, the more this deformation can be neglected. The condition of a large indentation depth d into a ductile material is met using a wedge of hardened steel, pressed $d = 200$ μm into titanium.
- No intermediate layer between the diamond coating and the titanium substrate is modelled since Vlassak's system shows a sharp chemical transition between coating and substrate.
- Experimentally, delaminated pieces of the coating become separated from the sample (Vlassak, 1997). Also, within the framework of this paper it was not possible to model cracks or crack growth. The finite element analyses are designed as static analyses. Therefore, only the still-attached part of the coating—as a 'snap shot'—in the domain $x > w$ is being considered. This corresponds to setting $w_2 = 0$ in eqn (6).

The two-dimensional finite element mesh is mainly built on eight-noded isoparametric plane strain elements with reduced integration. Around the contact area nine-noded hybrid elements are used to get a good simulation of the plastic incompressibility. The contact is modelled using contact elements for the sample and a rigid surface for the wedge.

Because of the symmetry, only half of the problem is modelled. The dimensions of the substrate are (Δx: 8304 μm, Δy: 4144 μm). The bottom of the specimen is constrained in the y-direction, the side can move freely. The coating of thickness $t = 2$ μm reaches from $x = w$ to $x = 8304$ μm. The number of the elements varies between 4260 (no coating) and 5581 ($w = 500$ μm). Fig. 3 shows the finite element mesh and a sketch of the relevant geometry.

For metals it is often true that the Tresca and von Mises flow criteria give similar predictions for the deformation. It is assumed that this also holds for titanium. Thus, the titanium substrate is modelled as an elastic-plastic solid with a von Mises flow criterion without strain hardening and using $E = 117$ GPa, $v = 0.31$ and $Y = 732$ MPa, in accordance with material data from Vlassak (1997). The diamond coating is linear elastic with $E = 1000$ GPa and $v = 0.25$.

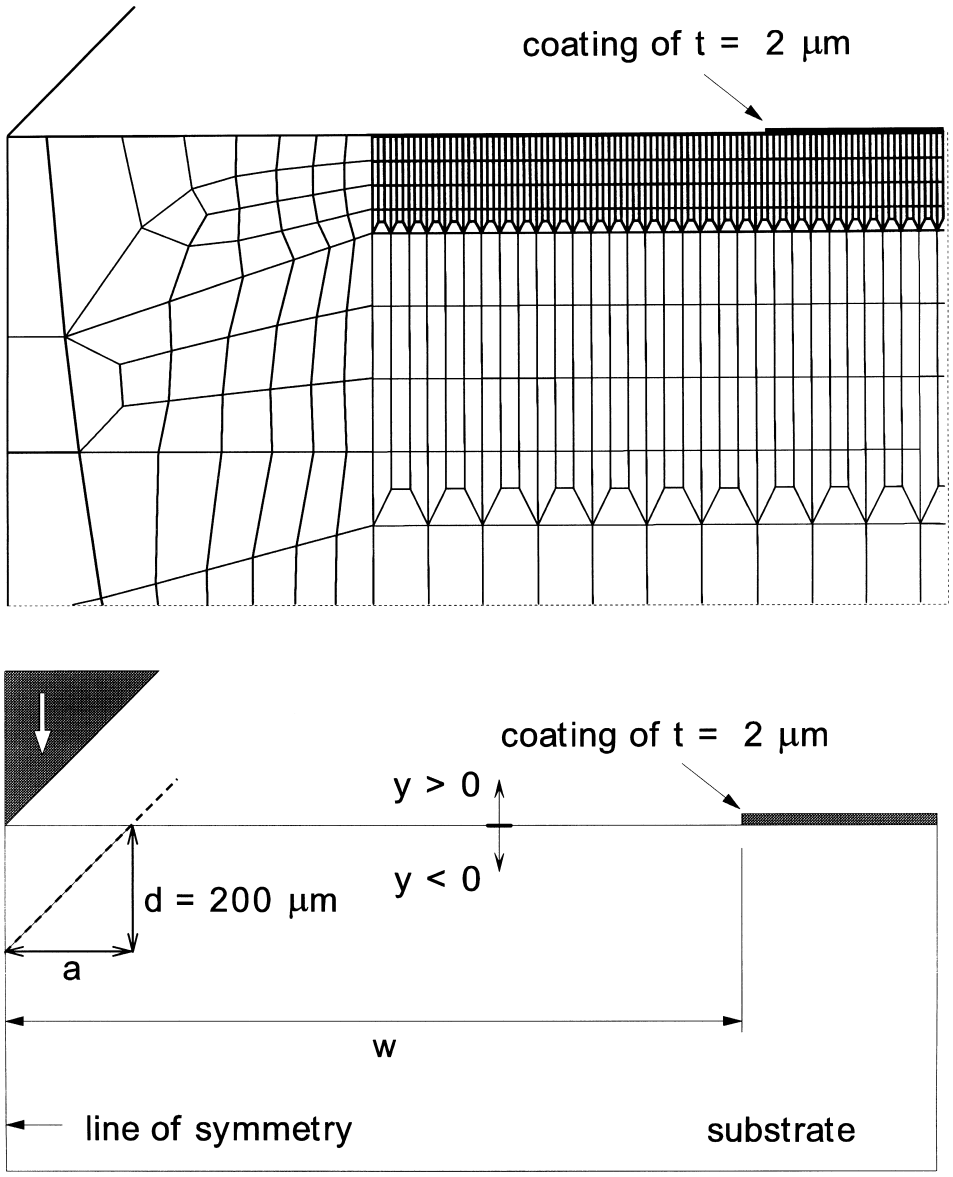

Fig. 3. Finite element mesh (above) and sketch of it (below). The elements of the coating are at $y > 0$.

The wedge shows an inclination of $\beta = 45^\circ$ and no tip blunting. To simulate an indentation it is pressed $d = 200$ μm into the specimen (see Fig. 3), which is then analyzed under load. For a comparison with the analytical model the effect of friction is being neglected.

The simulations for a coated substrate are performed for different values of the beginning of the coating, at $x = w$. It is assumed that the deformation of this system is similar to the deformation of a system where crack growth would have been incorporated. This is a good approximation considering that the energy used for plastic deformation is much smaller than the energy stored within the coating.

Finite element simulations of the wedge indentation test have been performed by Jayadevan and Narsimhan (1995). There, a rigid wedge of an inclination angle $\beta = 45^\circ$ was pressed into a soft uncoated copper sample of $E = 100$ GPa, $\nu = 0.3$, $Y = 200$ MPa, and a very low linear isotropic hardening with a tangent modulus of 10 MPa. Four-noded quadrilateral plane-strain elements were used for the substrate while the wedge is described as a frictionless rigid line. For the substrate a re-meshing algorithm was used. The dimensions of the substrate and the boundary conditions are similar to our case, as is the indentation depth of 180 μm.

3. Results

3.1. Uncoated substrate

In this section the simulated deformation behavior of an uncoated substrate is compared with the analytical solutions used by Vlassak (1997). Fig. 4 shows the deformed finite element mesh of the substrate around the indentation area. Below the indenter the finite elements are strongly deformed. A pile-up at the edge of contact is created so that the contact width is a ≈ 275 μm (instead of 200 μm without pile-up).

The deformation behavior is in good agreement with Jayadevan and Narsimhan (1995), especially in some distance from the contact area. In both cases, the pile-up is significantly sloped from the rim of the contact to about twice the contact width. While the pile-up in Jayadevan and Narsimhan (1995) shows a relatively constant slope of an angle of approx. 12°, the pile-up in our calculation exhibits an angle of about 25° near the rim of the contact and of about 6° further away from it (see Fig. 4). This

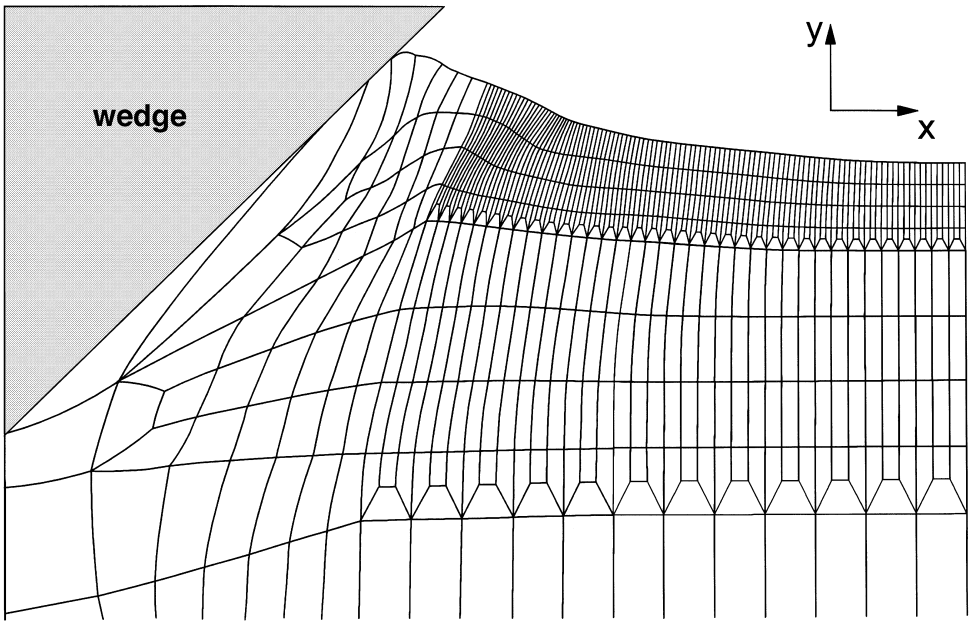

Fig. 4. Deformed finite element mesh of the uncoated substrate. The corresponding undeformed mesh is analogous to Fig. 3 without coating.

might be explained by the different element formulation (i.e. eight-noded vs four-noded elements), the different meshing (i.e. number and size of elements, and the use of a re-meshing technique), and the different material data of the specimen. However, the effects caused by the element characteristics are less significant further away from the contact area because of the smaller deformation of the elements. This applies to the distances of $x \geqslant 500$ μm where the coatings begin. A slight oscillation of the shape of the pile-up is in agreement with Jayadevan and Narsimhan (1995).

To compare our results to the analytical model, the effective contact width a_{eff} is calculated from the finite element computation and then used as an input parameter for the analytical model. Then the analytical calculation is compared to the directly evaluated (numerical) results from the finite element simulation.

Two methods to calculate a_{eff} are considered:

1. A pile-up volume $V_{\text{pile-up}} = 11{,}435$ μm^3 from the finite element mesh is calculated using the condition $y > 0$ and a width of the specimen of $\Delta z = 1$ μm. Applying eqns (9) and (10) with a displaced volume of $V_o = 20{,}000$ μm^3 yields $a_{\text{eff}} = 131$ μm and a radius of the plastic zone of $c \approx 963$ μm.
2. The radius c of the plastic zone is evaluated directly by extracting the von Mises equivalent stress at the surface nodes. It follows a radius $c \approx 750$ μm and, using eqn (9), $a_{\text{eff}} = 102$ μm.

Experimentally, Vlassak measured $V_{\text{pile-up}} = 38 \pm 2\%$ V_0. Using this number with $a = 200$ μm from the analytical model one gets $a_{\text{eff}} = 157$ μm and $c = 1156$ μm.

The values of a_{eff} calculated in methods (i) and (ii) differ significantly from each other and from the experimental result. To explain these differences the finite element simulation and the experiment are compared first.

The finite element analysis with $V_{\text{pile-up}} = 0.57$ V_0 shows a larger pile-up than the experiment. This can be explained as follows:

- The finite element model does not incorporate strain hardening, in accordance with Vlassak (1997). If the titanium would exhibit strain hardening, it would reduce the pile-up (Tabor, 1951).
- The indentation is simulated without friction, in accordance with the analytical model. Friction also reduces the pile-up: a finite element simulation with a constant friction coefficient of 0.3 showed that the pile-up volume is reduced to 6200 μm^3, which is equivalent to $a_{\text{eff}} = 166$ μm. The value of $V_{\text{pile-up}} = 0.31$ V_0 is in satisfactory agreement with the experimentally measured $V_{\text{pile-up}} = 0.38$ V_0.

One object of our paper is to examine the effect of the presence of a coating compared to results from the analytical model. The analytical model can approximately incorporate the effect of strain hardening by replacing the yield stress in eqn (9) with an average strain in the plastic zone but there do not exist more data of the titanium samples from Vlassak (1997) to construct a more realistic finite element model. Also, the analytical model does not incorporate the effect of friction. Because of these different indentation conditions, the effects of friction and strain hardening are not examined further.

Considering a_{eff} from the finite element calculations—without friction and strain hardening—there exists a difference in the effective contact width of (i) and (ii). A possible explanation is that eqn (10) is too simple and thus the accuracy of the analytical model is limited in case of a large pile-up. A more extensive analysis of this problem is not possible within the context of this paper. Thus, the analytical solutions using a_{eff} from both methods (i) and (ii) are compared to the directly evaluated finite element solutions.

In Fig. 5. the (radial) strain ε_{xx} on the surface of the substrate is plotted vs the x-coordinate. The plastic zone extends up to $x \approx 700$ μm for the finite element simulation. There the directly evaluated finite element solution drops faster towards zero than the analytical solutions using $a_{\text{eff}} = 102$, 131 and 157 μm as an input parameter. In the elastic region the strains are converging. Using $a_{\text{eff}} = 102$ μm gives smaller compressive strains than the finite element solutions; $a_{\text{eff}} = 157$ μm yields a higher compression.

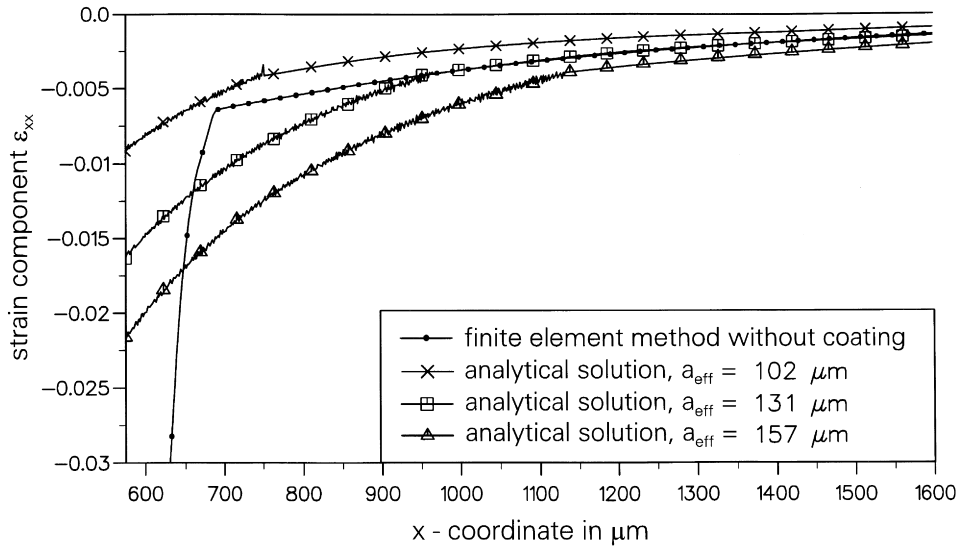

Fig. 5. Strain ε_{xx} vs x in μm for the analytical solutions and the finite element solution.

The best agreement with the finite element calculation is reached using $a_{\text{eff}} = 131$ μm in the domain 950 $\mu\text{m} \leqslant x \leqslant 1400$ μm.

Thus, if the pile-up is determined with reasonable accuracy then—for certain ranges—the analytical model using $a_{\text{eff}} = 131$ μm from method (i) shows a very good agreement with the direct finite element solution. This seems to be surprising since the plastic radius c from method (i) is too large with respect to the direct finite element result (see method (ii)). It seems to be the case that for our problem the analytical model gives slightly too small values of $|\varepsilon_{xx}|$ if the plastic radius c is given. The two tendencies of a too large plastic radius c and too small compressive strains for a given c appear to cancel each other and so a good agreement is reached.

Fig. 6 shows ε_{xx} for larger x. Above $x = 1700$ μm, the directly evaluated ε_{xx} is decreasing faster toward zero than the analytical solutions. Between $x = 2100$ μm and $x = 2500$ μm the agreement with the analytical solution using $a_{\text{eff}} = 102$ μm is very good. Only for $a_{\text{eff}} = 157$ μm there is no satisfactory correspondence to the finite element solution, the analytically calculated strains in the elastic region are always significantly more compressive.

Using ε_{xx} and Hooke's Law, one can calculate the strain energy density W_1 and, under the assumption $W_2 = 0$, the energy release rate G (eqn (6)), and also the total strain energy E_{tot} stored in a coating that extends from w to ∞:

$$E_{\text{tot}}(w, a_{\text{eff}}) := t\,\Delta z \int_{w}^{\infty} W_1 \,\mathrm{d}x. \tag{11}$$

The width Δz of the specimen can be chosen arbitrarily because of the plane strain condition. Fig. 7 shows the analytically calculated diagram of E_{tot} vs w for different values of the effective contact width and $\Delta z = 1$ μm. The energy E_{tot} varies significantly with $a_{\text{eff}} = 157$ μm, giving considerably larger values than $a_{\text{eff}} = 102$ μm and $a_{\text{eff}} = 131$ μm. This furthermore shows that a precise determination of the radius c of the plastic zone is needed to make accurate predictions of the energy release rate. Vlassak (1997) has appreciated this strong dependence from a_{eff} and dedicated much work into experimentally determining the pile-up.

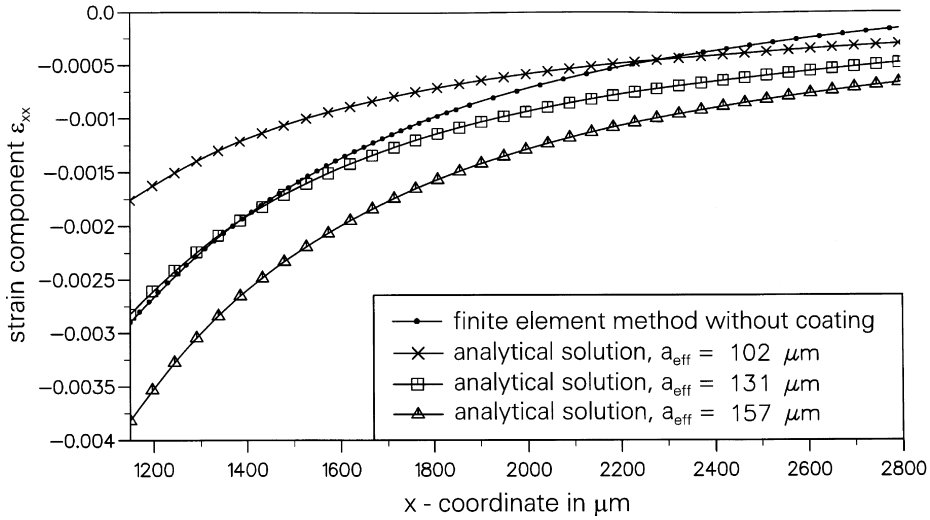

Fig. 6. Strain ε_{xx} vs x in analogy to Fig. 5 but for $1150 \leqslant x \leqslant 2800$ μm.

Because of the different indentation condition with respect to the analytical model, resulting in the small pile-up and thus the large a_{eff} compared to a_{eff} from the methods (i) and (ii), the analytical solution using $a_{\text{eff}} = 157$ μm from the experimental data is not considered further in the next sections.

From this section we may draw the following conclusions:

- The finite element analysis shows a large pile-up in accordance with the experiment. The differences in the deformation behavior can largely be explained by friction and strain hardening.
- The values of the radius c of the plastic zone determined from the analytical and the numerical calculations are singnificantly different. A possible explanation for this difference is that the incorporation of the pile-up into the analytical model is too simple. Nevertheless, the agreement

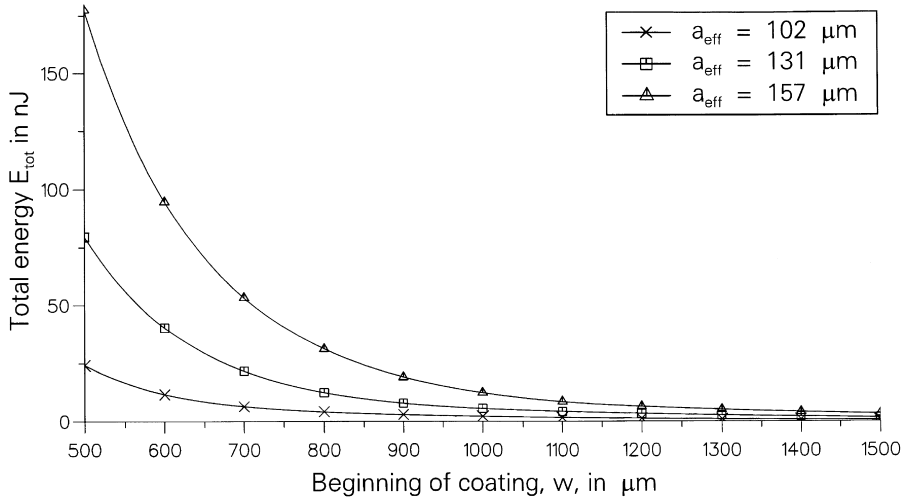

Fig. 7. Total strain energy E_{tot} within a coating vs w.

between numerical values and analytical values is very good at different distances from the point of first contact for $a_{\text{eff}} = 102$ μm and $a_{\text{eff}} = 131$ μm.

3.2. Coated substrate

In this section the consequences of a thin hard coating attached to the substrate will be examined. The deformation of the coated specimen in the vicinity of the contact area is similar to the deformation of the uncoated substrate. But around the coating the deformations are significantly altered (Fig. 8). Below the coating the substrate is less piled-up than in the uncoated region. This is because the hard coating resists deformation more than the softer, ductile substrate and holds it back. Since the displaced volume must be conserved the substrate is more strongly piled-up in front of the coating. Additionally, the finite elements are more strongly compressed in the radial (x-) direction in front of the coating than along the interface. Both effects are more heavily emphasized for $w = 500$ μm than for $w = 600$ μm (Fig. 8).

The bending of the coating—and therefore the existence of a stress gradient over the coating thickness—and also the piling up of the substrate right in front of the coating are not taken into account by the analytical model where only a compression in the x-direction is included. However, by looking at the deformation in the x-direction alone one can see a constraining effect of the coating. Because of this, the analytical model is considered with the help of the finite element method for different values of w.

In order to do this, the strain component ε_{xx} is plotted against the x-coordinate for $w = 680$ μm and compared to the finite element result and the analytical calculations for the uncoated substrate (Fig. 9). If the specimen is modelled with a coating, the strain ε_{xx} is altered significantly. At a small distance in front of the coating $|\varepsilon_{xx}|$ increases with respect to the uncoated specimen while $|\varepsilon_{xx}|$ below the coating decreases. $|\varepsilon_{xx}|$ reaches a local minimum at a short distance from the beginning of the coating, and then converges to the values of the uncoated substrate. Different values of w exhibit a qualitatively similar behavior. The larger the value of w, the smaller is the rapid change in strain.

This shows that the deformation state of the uncoated material can be used to describe coated materials only in an approximative way. Even if the deformation of the uncoated substrate could be calculated exactly by an analytical model, the reduced compression below the coating would not be correctly predicted. Below a hard coating the compressive strain ε_{xx} in the interface will be smaller than

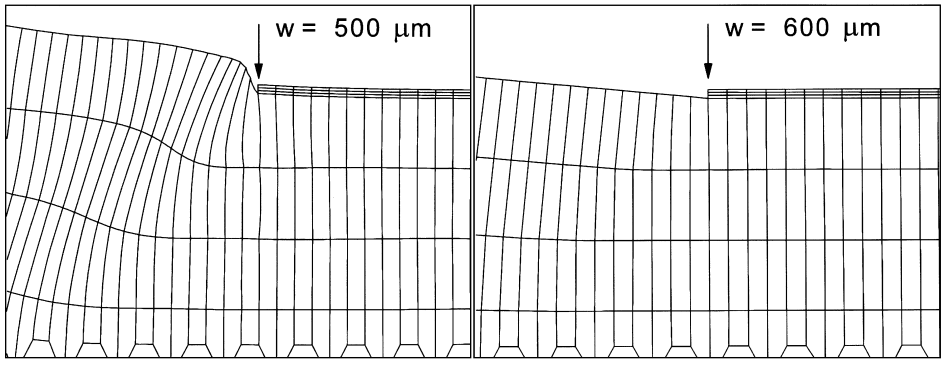

Fig. 8. Deformed finite element meshes in the vicinity of the beginning of the coating.

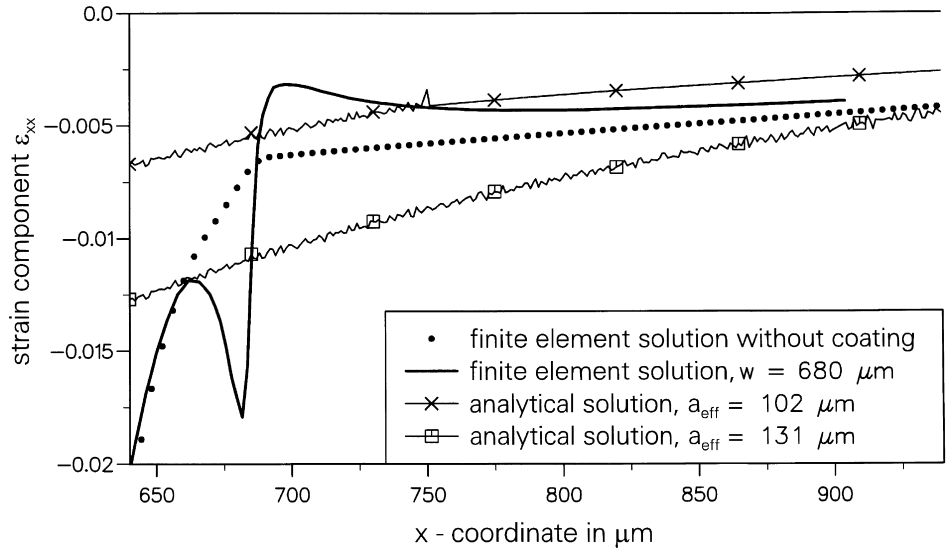

Fig. 9. Strain ε_{xx} along the interface vs x-coordinate.

for uncoated materials due to the constraining effect of the coating. This deviation is more heavily emphasized near the beginning of the coating and negligible at some distance from it.

For $w = 600$ μm, Fig. 10 shows the stress component σ_{xx} at the interface and at the surface of the coating. At the beginning of the coating at $x \approx 606$ μm (deformed) there exists a large difference between σ_{xx} along the interface and at the surface. This is caused by the bending of the coating so that the coating is differently strained on the upper and the lower side. Additionally, the boundary conditions are different at the left side of the coating at $x = w$, i.e. $\sigma_{xx}|_{\text{surface}} \equiv 0$ and $\sigma_{xx}|_{\text{interface}} \neq 0$.

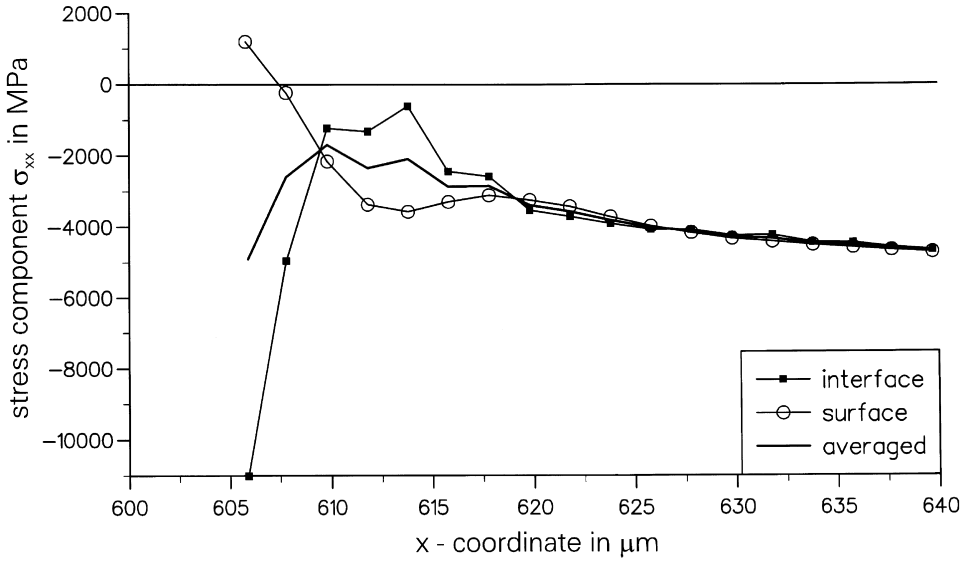

Fig. 10. Stress σ_{xx} along the coating vs x-coordinate of the deformed system.

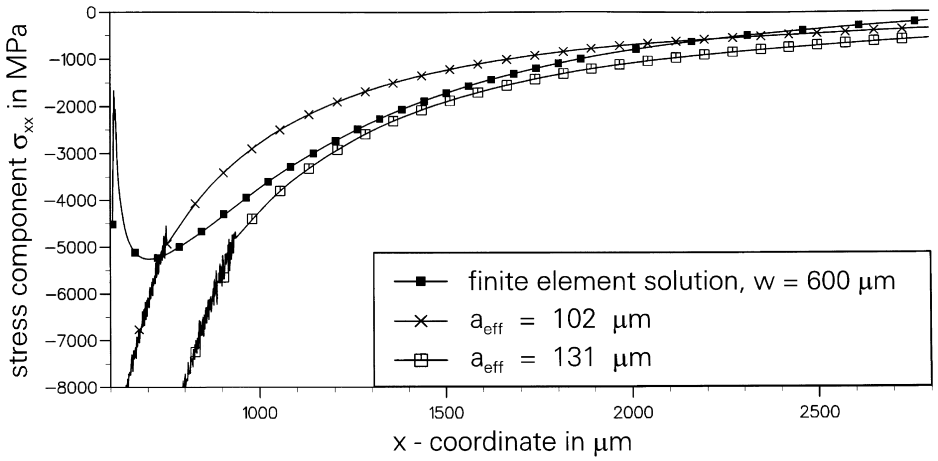

Fig. 11. Stress σ_{xx} vs x-coordinate.

From a distance $\Delta x \approx 12$ μm beyond the beginning of the coating the two stresses are virtually identical, so that the assumption from Section 2 that the stresses are constant over the coating thickness is validated by the finite element method. The region over which a large stress gradient exists in the coating is small compared to the extent of the coating itself ($\Delta_x \approx 7500$ μm). Also, this gradient gets smaller with larger w.

Also, the stresses σ_{xy} and σ_{yy} are significant only at the beginning of the coating, with σ_{yy} being very small at the interface. The assumption of the analytical model that the coating is simply compressed in the x-direction is therefore valid for most of the coating.

We now compare the averaged stress component σ_{xx} vs x for the finite element solution and the analytical solution for $w = 600$ μm (Fig. 11). Below $x \approx 700$ μm (see also Fig. 10) the absolute stresses are much smaller for the finite element calculation than for the analytical solutions. Their qualitative behavior for $x \geqslant 700$ μm is in accordance with the behavior of ε_{xx} in Fig. 9. As for ε_{xx}, the finite element result is nearer to the analytical calculation using $a_{\text{eff}} = 131$ μm at small x, whereas it is in better agreement with $a_{\text{eff}} = 102$ μm for $x > 2000$ μm. However, quantitatively the free surface of the coating leads to stresses that are lower than expected by simply using the strains and applying Hooke's Law. This effect can be seen clearly by considering the finite element solution within 1200 μm $\leqslant x \leqslant 1500$ μm. There the values of ε_{xx} for a coated and uncoated substrate have nearly converged, and ε_{xx} is in excellent agreement with $a_{\text{eff}} = 131$ μm (see Fig. 6) but the stress σ_{xx} is significantly lower.

Unfortunately, the gradient of σ_{xx} over the coating thickness t and the non-zero values of σ_{xy} and σ_{yy} at the beginning of the coating have the consequence that the energy release rate G can not be determined using Eq. (6), because there $\sigma_{xx} =$ constant over t, $\sigma_{yy} = 0$, and $\sigma_{xy} = 0$ is assumed. Thus, the numerical simulation shows that the analytical model does not give a realistic picture of the stress state at the beginning of the coating. Therefore it is preferable to compare the total stored energy within the coating E_{tot}. Because of the integration over x by calculating E_{tot} using Eq. (11), the influence of the stress variation at the beginning of the coating is suppressed.

To determine E_{tot}, the strain energy density $W = \frac{1}{2}\sigma_{ij}\varepsilon_{ij}$ is evaluated at each nodal point along the interface and the surface of the coating. Then, W is integrated over x for the interface and the surface separately. After averaging over the, virtually identical, values of the interface and the surface, this is

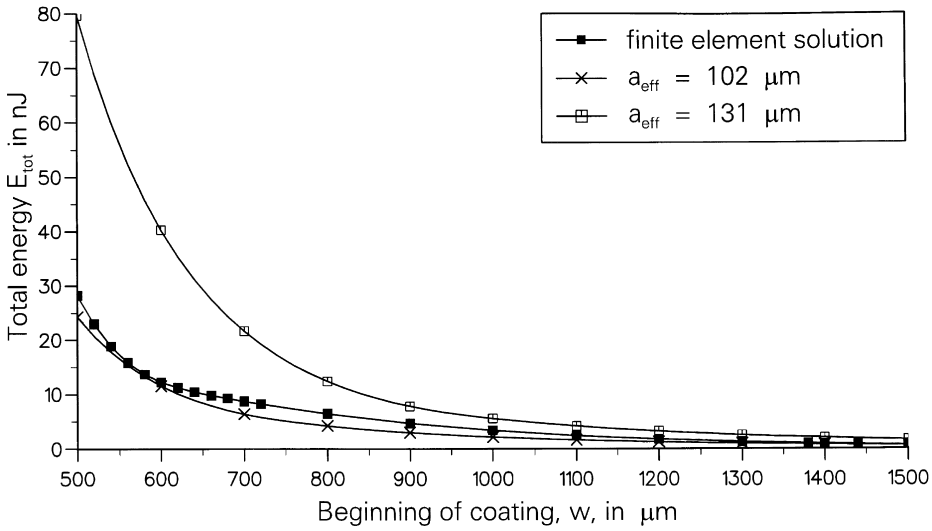

Fig. 12. Numerically and analytically calculated total energy E_{tot} vs w.

multiplied by the coating thickness $t = 2$ μm (t remains nearly constant, irrespective of the deformation) and an arbitrary width $\Delta z = 1$ μm.

Only the component (σ_{xx} ε_{xx}) gives a significant contribution to the energy E_{tot}. The other components are smaller than 0.3% of (σ_{xx} ε_{xx}) from $w = 600$ μm on. Even for $w = 500$ μm, where there exists a large bending of the coating, the other components do not exceed 5% of (σ_{xx} ε_{xx}). This is a further justification that the assumption of Vlassak's model is well obeyed, i.e. that the coating is only compressed in the x-direction.

Fig. 12 shows the total strain energy E_{tot} within the coating, plotted against the starting point w of the coatings (each data point representing one finite element calculation for a particular value of w). The finite element solution and the analytical solution using $a_{\text{eff}} = 102$ μm are in good agreement, the difference for $w < 1500$ μm being smaller than 37%. Using $a_{\text{eff}} = 131$ μm on the other hand gives much larger values of E_{tot}. This might look surprising at first since the agreement in the strains and stresses is comparatively good over certain regions. But at the beginning of the coating the numerically calculated strains and stresses are much smaller due to the boundary conditions of the coating (see Figs. 9 and 10) and also at larger distances from the indentation ($x \geqslant 2000$ μm). By multiplying ε_{xx} and σ_{xx} and integrating over x these two effects are incorporated in lowering E_{tot} of the finite element solution in comparison to $a_{\text{eff}} = 131$ μm. For larger w, Fig. 13 shows the development of E_{tot}. From $w \geqslant 1600$ μm on the numerical calculation is always smaller than both analytical calculations. Thus the agreement between the numerical solution and $a_{\text{eff}} = 102$ μm is always better than for $a_{\text{eff}} = 131$ μm. This behavior can not be deduced from considering ε_{xx} alone.

Fig. 14 shows the relative difference in E_{tot} between the analytical calculations and the numerical simulation in percent with respect to the numerical simulation. The values for E_{tot} using $a_{\text{eff}} = 131$ μm are at least 60% larger than the finite element results with the minimal deviation appearing at $x = 1000$ μm. The difference between the finite element solution and $a_{\text{eff}} = 102$ μm on the other hand does not exceed $\pm 50\%$ for $w \leqslant 1800$ μm. It ranges from only -28.5 to $+25.5\%$ for 1200 μm $\leqslant w \leqslant 1700$ μm. In both cases the difference increases for large w and reaches over 1000% at $w = 2900$ μm for $a_{\text{eff}} = 131$ μm, and over 300% at $w = 2900$ μm for $a_{\text{eff}} = 102$ μm.

The very good agreement between the finite element solution and $a_{\text{eff}} = 102$ μm again shows that the

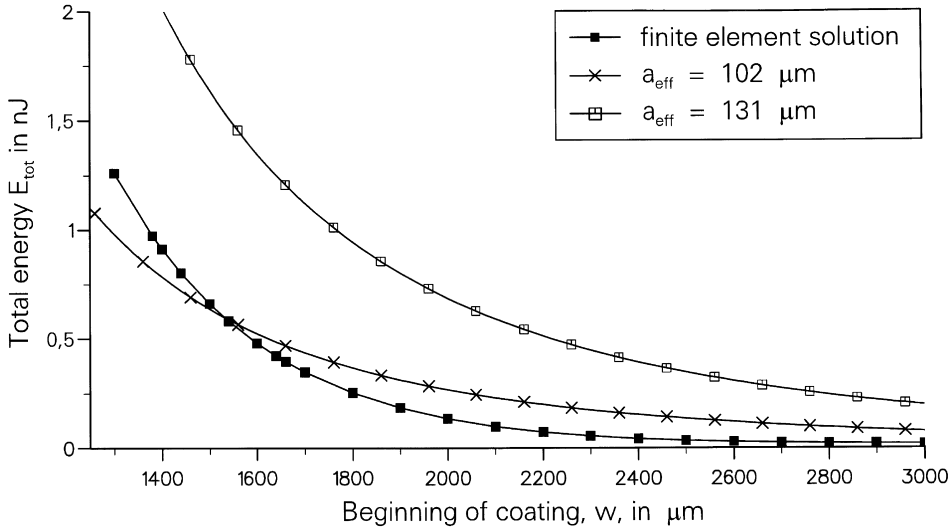

Fig. 13. E_{tot} vs w in analogy to Fig. 12 for $1250 \leqslant w \leqslant 3050$ μm.

analytical model used by Vlassak (1997) can—if used with care—be applied to more realistic wedge indentations despite its limitations. Thus, with the help of Fig. 14 one can estimate the range of w, within which a certain analytical model is in agreement with the more realistic finite element model for a chosen range of accuracy.

Vlassak (1997) found experimentally that the ratio of the extent of the delaminated area and the contact width, w/a, is approx. 5–6 for different value of the indentation depth. With $a = 275$ μm from the finite element simulation this gives a beginning of the coating w from 1375 μm to 1650 μm. In this range the agreement for E_{tot} of the finite element simulation with the analytical solution using $a_{eff} = 102$ μm is best.

It should be noted, though, that experimentally less pile-up had occurred than predicted by the finite

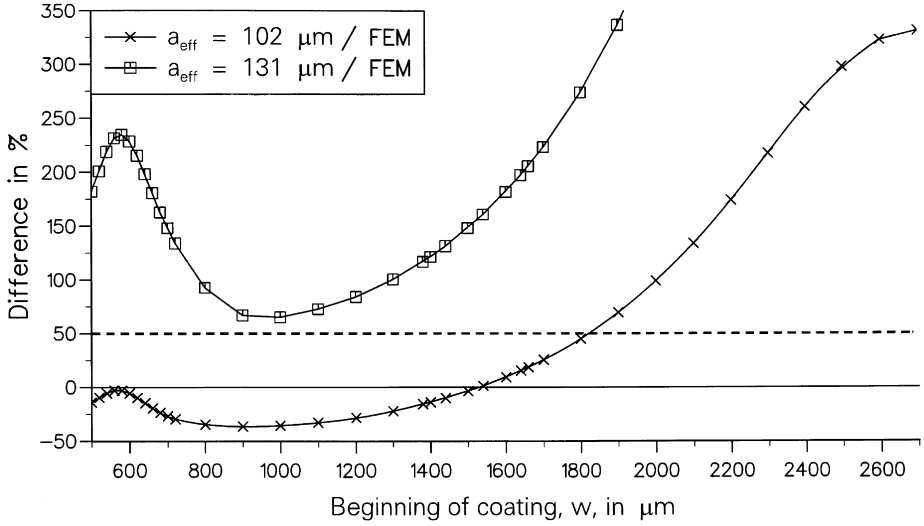

Fig. 14. Relative differences of E_{tot} vs w. The range of $\pm 50\%$ difference is plotted as a dashed line.

element model. If Vlassak (1997) had had the amount of pile-up given by the finite element model, the debond would probably not have extended so far away from the indenter.

For the energy release rate, G, on the other hand, the finite element model shows that the assumptions of the analytical model are not met. However, it may be possible to resolve this problem. Using the finite element method we calculate a (finite) energy release rate G^*:

$$G^* := -\frac{1}{\Delta z}\left(\frac{\Delta E_{\text{tot}}}{\Delta w}\right).$$

Here, $(\Delta E_{\text{tot}}/\Delta w)$ denotes the numerical differentiation of the finite data points of the (E_{tot} vs w)—plot in Figs. 12 and 13. This is in analogy to the analytically defined energy release rate G of eqn (6) under the assumption that delaminated parts of the coating are also detached from the still adherent part of the coating (i.e. $W_2 = 0$). It is equivalent to the picture of an observer who does not follow the process of the coating delamination but only measures the initial and the final state of the specimen. The definition of G^* therefore follows from simple energy calculations without consideration of crack tip fracture mechanics methods. For small enough Δw, though, G^* should be virtually identical to G.

The resulting (G^* vs w)—plot is shown in Fig. 15. For $w > 560$ μm, G^* again shows good agreement between the finite element calculation and $a_{\text{eff}} = 102$ μm. Using $a_{\text{eff}} = 131$ μm on the other hand overestimates the finite element values much more strongly for $w < 1000$ μm. For the range $w \geqslant 1200$ μm, Fig. 16 shows the corresponding G^*—w-diagram. For $w = 1200$ μm the finite element result is between the two analytical results and approaches $a_{\text{eff}} = 102$ μm for higher w.

For the experimentally measured ratio $w/a \approx 5$–6, corresponding to $1375 \leqslant w \leqslant 1650$ μm, the analytical solution of G^* using $a_{\text{eff}} = 102$ μm differs between -46 and $+32\%$ with respect to the finite element calculations, whereas $a_{\text{eff}} = 131$ μm gives differences that range between 42% and 75%. Thus the differences are significant but the values of G^* are within the same order of magnitude. Furthermore, the graphs have a similar shape so that if an appropriate a_{eff} is chosen, the agreement could be very good. In our case chosing $a_{\text{eff}} = 102$ μm is an appropriate choice for calculating E_{tot} and G^* while using $a_{\text{eff}} = 131$ μm is in better agreement with the strains and stresses at 1375 μm $\leqslant w \leqslant 1650$ μm.

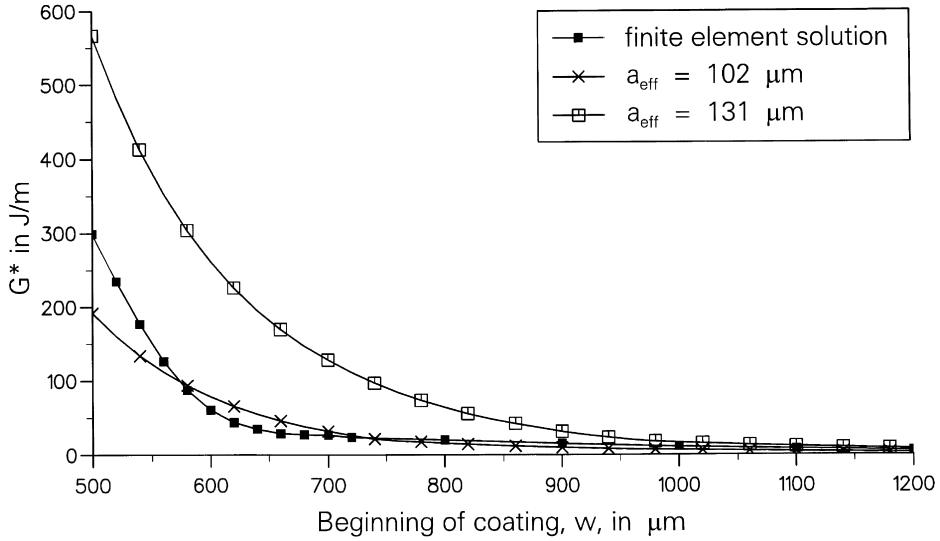

Fig. 15. G^* vs w for $500 \leqslant w \leqslant 1200$ μm.

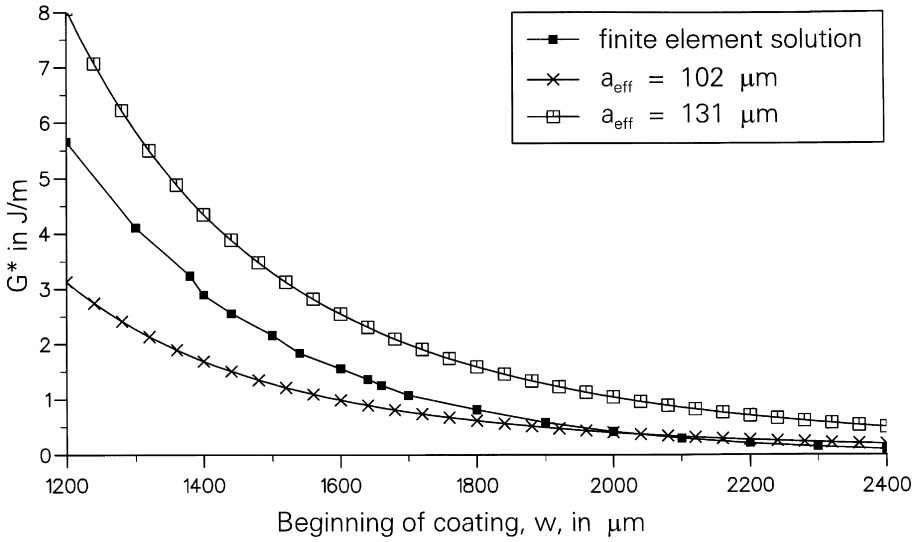

Fig. 16. G^* vs w for $1200 \leqslant w \leqslant 2400$ μm.

A possible explanation for the good agreement in G^* is the following: the finite element model shows that there is a stress gradient at the beginning of the coating. If we cut out a piece of the coating of length Δw from the beginning of the coating at $x = w$, we would not simply remove the stresses over the same length. Rather we would shift the area of the stress gradient to a location $w + \Delta w$ at the new edge. That means that (apart from a small reduction in the magnitude of the gradient) the state at the beginning of the coating remains intact and we have effectively 'cut out' a part of the gradient free section from the stress plot. This scenario differs from the analytical model where G is only dependent of the stress state at the crack tip.

It must be stressed again that G^* is not calculated from crack tip fracture mechanics assumptions. Therefore, the local stress field is important only to obtain E_{tot} and the change in the strains and stresses during the growth of a delamination is not addressed. However, the energy release using the analytical model is reasonably accurate even though the finite element calculations show that the strain and the stress fields are much more complicated than those given by the analytical model.

Through an extension of the existing finite element mesh one could model a crack along the interface and in a further step one could model crack growth. By doing this, one could include the substrate deformation and the stress distribution within the coating more accurately. Furthermore, a direct evaluation of G from the finite element simulation would be within reach. Such an advanced simulation is possible but it would take a much larger effort to construct the finite element mesh and also a significant effort to program the material behavior (condition for crack growth, etc.). This goes well beyond the scope of the present paper.

But using the finite element method, even with relatively simple assumptions, it is possible to obtain a good approximation of the deformation and the resulting stress field and also a good estimate of the energy release rate G^* within the sample.

From this section the following conclusions may be drawn:

- The presence of a coating significantly lowers the strains in the interface around the beginning of the coating. This decrease means that even if the strains of an uncoated specimen could be calculated exactly the strain component ε_{xx} of a realistic coated system could not be described near the

beginning of the coating.

At larger distances from the indentation the finite element solution converges to the solution for the uncoated specimen.

At the beginning of the coating the bending creates a stress gradient over the coating thickness t. Also the free edges of the coating cause a difference in stress at the interface and the surface. At a larger distance from the indentation the stresses given by the finite element solution are smaller than they would be if calculated from the given strains by using Hooke's law, due to surface effects. The complex stress state makes a calculation of the energy release rate G impossible without more advanced finite element modelling, provided the stresses are to be used directly.

- The numerically calculated total energy E_{tot} in the coating is in good agreement with the analytical values using $a_{\text{eff}} = 102$ μm up to $x \approx 1800$ μm because the attachment of a coating tends to lower the strains and stresses within the interface with respect to the uncoated system.
- The calculation of a released energy G^* leads to a good agreement between the numerical values and the analytical values using $a_{\text{eff}} = 102$ μm. It shows that the analytical model gives realistic values of the energy release although the strains and stresses in the vicinity of the beginning of the coating are not described properly.

4. Conclusions

The object of this work was to investigate the effect of the presence of a thin hard coating on the deformation behavior of a soft substrate subjected to wedge indentation. To do this, finite element calculations have been performed to obtain a realistic picture of the deformation and the stress state within the specimen. These calculations have been compared to an analytical model used by Vlassak (1997).

It was possible to show that the analytically calculated strains within the surface of an uncoated specimen can be in very good agreement with the finite element results for certain ranges of the distance from the indentation but are quite different for others. The (partial) agreement is good if the effective contact width a_{eff} that incorporates pile-up is chosen in such a way that the realistic value of the radius c of the plastic zone from the finite element model is matched closely.

If a coating is applied, the coating is less compressed than the uncoated substrate at the beginning of the coating but converges to the uncoated solution further away from it. This means that in general ε_{xx} can not be described using the analytical solution for an uncoated specimen.

The finite element calculations also showed that the stress component σ_{xx} exhibits a large stress gradient at the beginning of the coating, contrary to the assumptions of the analytical model. Also other stress components are present. These effects prohibit a calculation of the energy release rate G from this stress field. The directly evaluated stress component was in much better agreement with the analytical solution for regions further away from the beginning of the coating.

When the total energy E_{tot} stored in the coating was calculated, the agreement was good between the finite element results and the analytical values for $a_{\text{eff}} = 102$ μm up to $x \approx 1800$ μm. Although in this range of x the analytical solution of the strains and stresses using $a_{\text{eff}} = 131$ μm was closer to the finite element model the presence of a coating reduces E_{tot} with respect to the analytical model.

By defining an energy release rate G^* it was possible to find a measure of the released energy per coating delamination Δw. This method suppressed the effect of the stress gradient and the presence of the other stress components and relied only globally on the stress field within the coating. It followed that the analytically and numerically calculated energy differences are significantly different but of the

same magnitude. A very good agreement was reached between the finite element solution and the analytical solution using $a_{\text{eff}} = 102\ \mu\text{m}$.

In this paper is was therefore possible to show that despite its disadvantages the analytical method for the wedge indentation test gives useful results. These results can be made more accurate by employing the finite element method and subsequently optimizing the input parameters of the analytical model for best agreement.

Acknowledgements

The first author wishes to thank the Fraunhofer-Institute fuer Werkstoffmechanik for its support and the Nix Group at Stanford University for discussions and help. The second author gratefully acknowledges financial support of the U.S. Department of Energy through DOE grant no. DE-FG03-89ER45387.

References

Bathe, K.H., 1986. Finite-Elemente-Methoden. Springer, Heidelberg.
Drory, M.D., Hutchinson, J.W., 1994. Diamond coating of titanium alloys. Science 263, 1753–1755.
Hill, R., 1950. The Mathematical Theory of Plasticity, Oxford Engineering Science. Oxford University Press, Oxford.
Jayadevan, K.R., Narsimhan, R., 1995. Finite element simulation of wedge indentation. Int. J. Comp. Struct. 57 (5), 915–927.
Johnson, K.L., 1970. The correlation of indentation experiments. J. Mech. Phys. Solids 18, 115–126.
Mittal, K.L., 1995. Adhesion Measurement of Films and Coating: A Commentary. VSP, Utrecht, pp. 1–13.
Schulze, M., 1996. Untersuchungen zur Charakterisierung mechanischer Eigenschaften von Schichten. IWM-Bericht W2/96, Fraunhofer-Institut für Werkstoffmechanik (IWM), Freiburg.
Tabor, D., 1951. The Hardness of Metals. Oxford University Press, Oxford.
Timoshenko, S.P., Goodier, J.N., 1987. Theory of Elasticity. McGraw-Hill, New York.
Vlassak, J.J., Drory, M.D., Nix, W.D., 1997. A simple technique for measuring the adhesion of brittle films to ductile substrates with application to diamond-coated titanium. J. Mater. Res. 12, 1900–1910.
Zienkiewicz, O.C., 1977. The Finite Element Method. McGraw-Hill, UK.